How does the mode of evolutionary divergence affect reproductive isolation?

Bianca De Sanctis[1,2], Hilde Schneemann[1], John J. Welch[1]

[1] Department of Genetics, University of Cambridge, Cambridge CB2 3EH, UK.
[2] Department of Zoology, University of Cambridge, Cambridge CB2 3EJ, UK.

Abstract

When divergent populations interbreed, the outcome will be affected by the genomic and phenotypic differences that they have accumulated. In this way, the mode of evolutionary divergence between populations may have predictable consequences for the fitness of their hybrids, and so for the progress of speciation. To investigate these connections, we present a new analysis of hybridization under Fisher's geometric model. Unlike previous such analyses, we derive results using combinatorics, and so we make few assumptions about the additive and dominance effects that differentiate the hybridizing populations. Results show that the strength and form of postzygotic reproductive isolation (RI) depend on just two properties of the fixed effects, which we call the "total amount" and "net effect" of evolutionary change. It follows that identical patterns of RI can arise in different ways. Nevertheless, the key quantities do contain information about the history of divergence, and the dominance and additive effects contain complementary information. Our results also clarify the roles of large- and small-effect substitutions in generating RI. For example, when hybridizing populations are locally adapted, populations that adapted with a few large-effect mutations will show more intrinsic RI than populations that followed the same phenotypic trajectory, but with many small mutations.

Introduction

Genomic and phenotypic differentiation between populations is a major cause of reproductive isolation (RI), preventing hybrids from forming, or reducing their fitness when they do form. However, differentiation can also be a source of adaptive variation, if hybrids contain new fit combinations of traits or alleles, or act as conduits passing existing combinations from one population to another (Arnold and Hodges, 1995; Edmands, 1999, 2002; Coyne and Orr, 2004; Bierne et al., 2013; Schluter and Conte, 2009; Bernardes et al., 2017; Coughlan and Matute, 2020).

Which of these outcomes actually takes place must depend on the types of phenotypic and genomic differences that have accumulated. A fundamental challenge in evolutionary biology is to understand the connections between the mode of evolutionary divergence, the type of differences that accrue, and the outcomes of subsequent hybridization. What, for example, are the respective roles of large- versus small-effect mutations in causing RI, and what are the roles of natural selection versus genetic drift (Coyne and Orr, 2004; Jezkova et al., 2013; Satokangas et al., 2020; Moran et al., 2021)?

One tool to address these questions is Fisher's geometric model. This is a mathematical model of selection acting on quantitative traits (Fisher, 1930, Ch. 2), and has been used to understand both phenotypic data, e.g., QTL for traits involved in adaptive divergence (Orr, 1998), and fitness data. In the latter case, the phenotypic model need not be treated literally, but is a simple way of generating a fitness landscape (Martin and Lenormand, 2006; Martin, 2014). Both uses of the model have been applied to hybrids (Mani and Clarke, 1990; Barton, 2001; Chevin et al., 2014; Fraïsse et al., 2016; Simon et al., 2018; Yamaguchi and Otto, 2020; Schneemann et al., 2020; Thompson et al., 2021; Schneemann et al., 2022).

Most importantly here, the model allows us to consider the effects in hybrids of evolutionary changes of different sizes, and which were driven by different evolutionary processes (Hartl and Taubes, 1996; Orr, 1998; Simon et al., 2018; Schneemann et al., 2020). However, previous analytical results have depended on strong assumptions about the distribution of the fixed effects (e.g., normality, universal pleiotropy, and independence among traits) which greatly limits their generality and application. Furthermore, the results describe the overall strength of RI in terms of a single fitted parameter, whose relationship to the process of evolutionary divergence is obscure.

In this paper, we generalise previous work on Fisher's geometric model in two ways. First, we show how some previously published results concerning hybrid fitness (Schneemann et al., 2020) apply exactly, without making any assumptions about the distribution of fixed effects. We do this by deriving the results with combinatorics, instead of making parametric assumptions about the distribution of fixed differences. Second, we show how some key quantities which appear in the results relate transparently to the history of divergence between the parental populations. Finally, we use the results to clarify the different contributions of large- versus small-effect substitutions to overall RI.

1 Results

1.1 The model

Under Fisher's geometric model, the fitness of any individual depends solely on its values of n quantitative traits. The trait values for an individual can be collected in an n-dimensional vector $\mathbf{z} = (z_1, ..., z_n)$; and its fitness, w, depends on the Euclidean distance of this phenotype from an optimum $\mathbf{o} = (o_1, ..., o_n)$, whose value is determined by the current environment. We will assume the simplest form of the model, where the log fitness declines with the square of the distance:

$$\ln w = -\left\|\mathbf{z} - \mathbf{o}\right\|^2 = -\sum_{j=1}^{n}(z_i - o_i)^2 \tag{1}$$

This model can be derived either exactly, or approximately, from a wide class of more complicated fitness functions (Martin, 2014; Schneemann et al., 2020), and in these latter cases, only a few, if any of the n traits, need to be identified with real quantitative traits that might be measured in the field.

1.1.1 Characterizing parental divergence

Given this model, both mutations and fixed differences can be represented by n-dimensional vectors of change in the phenotypic space. We will consider hybrids between two diploid parental lines, denoted P1 and P2, which have accumulated D fixed genomic differences. Our major assumption about these differences is a lack of phenotypic epistasis, i.e. that effects on the phenotype are additive between loci (further confirming that the n traits might not be identifiable with standard quantitative traits). Given this assumption, each allele can be completely described via its additive and dominance effects on each trait. The additive and dominance effects can be collected in $D \times n$ - dimensional matrices, denoted $\mathbf{a} = (a_{ij})$ and $\mathbf{d} = (d_{ij})$, and we treat these as fixed observations, rather than random variables. For convenience, these effects are all defined relative to the P1 allele, whether ancestral or derived. This means that, for a single trait j and locus i, the homozygous state for the P2 allele is represented as $2a_{ij}$, the heterozygote as $a_{ij} + d_{ij}$, and homozygote for the P1 allele as 0. The trait vector or phenotype of P2 can therefore be written as P1 plus the sum of twice the additive effects. For any trait $j = 1, ..., n$, we have

$$z_{\mathrm{P2},j} = z_{\mathrm{P1},j} + 2\sum_{i=1}^{D} a_{ij} \tag{2}$$

Figure 1a shows an illustrative example with $n = 2$ traits, and $D = 5$ substitutions. Here, the black arrows represent the path of homozygous substitutions, $2\mathbf{a}$, leading from P1 to P2 via their most recent common ancestor (MRCA).

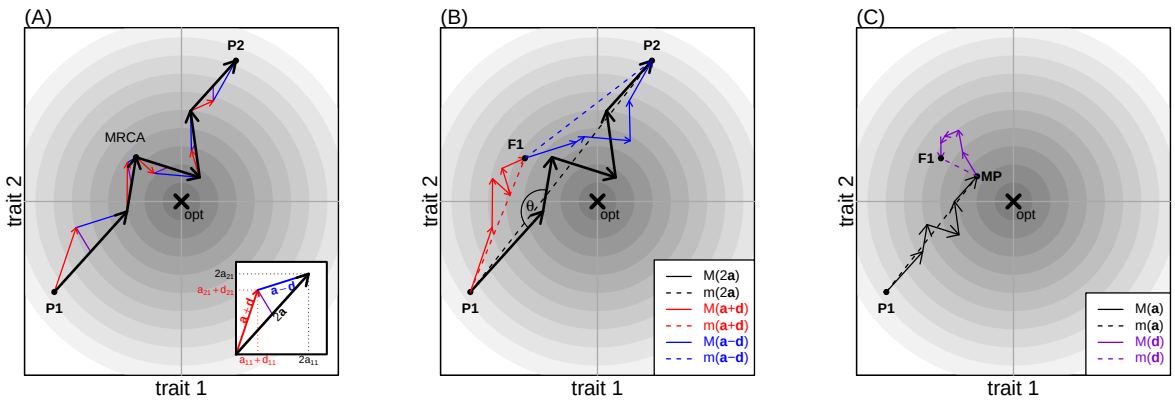

Figure 1: The key quantities for determining hybrid fitness under Fisher's geometric model. **(A)**: The fitness of any given phenotype is determined by its distance from some optimum phenotype, as determined by the current environment. This optimum and fitness landscape is illustrated, for $n = 2$ traits, by the cross and contour lines. The diploid parental lines, P1 and P2, are each associated with a phenotypic value, and are connected by a chain of $D = 5$ homozygous fixed differences, shown as black arrows. The model allows for phenotypic dominance, so that each homozygous substitution is composed of a pair of heterozygous effects, defined either from the P1 state (red arrows) or the P2 state (blue arrows), combining the additive effects (black) with the dominance effects (purple). **(B)**: the initial F1 hybrid is heterozygous at all divergent sites, and so its phenotype is found by combining the complete set of heterozygous effects. **(C)** The F1 can also be represented as the sum of the dominance effects (purple arrows), starting at the midparent (MP). **Inset panels**: The fitness of an arbitrary hybrid is affected by the *total amount of evolutionary change* (the sum of squared lengths of the arrows), and by the *net effect of the evolutionary change* (the squared lengths of the dotted lines). See Section 1.3.2 for full details.

Each homozygous substitution is composed of two heterozygous effects (see Figure 1A inset). The effect of inserting the ith P2 allele into a P1 background is $\mathbf{a}_i + \mathbf{d}_i$, and is shown as a red arrow in Figure 1. The effect of inserting the ith P1 allele into a P2 background is $-(\mathbf{a}_i - \mathbf{d}_i)$, and is shown as a blue arrow. In the initial F1 hybrid, all D of the divergent alleles are present in heterozygous state. As such, the F1 phenotype can be written in two ways.

$$z_{\mathrm{F1},j} = z_{\mathrm{P1},j} + \sum_{i=1}^{D} (a_{ij} + d_{ij}) \tag{3}$$

$$= z_{\mathrm{P2},j} - \sum_{i=1}^{D} (a_{ij} - d_{ij}) \tag{4}$$

This is illustrated in Figure 1B, where the path from either of the parental phenotypes to the F1 is found by combining the heterozygous effects (i.e. either the red or blue arrows). If we take the mean of eqs. 3-4, we can also think of the F1 in a third way – as the point which connects the chain of dominance effects, $\mathbf{d}$, to the midparental phenotype.

$$z_{\mathrm{F1},j} = \frac{z_{\mathrm{P1},j} + z_{\mathrm{P2},j}}{2} + \sum_{i=1}^{D} d_{ij} \tag{5}$$

This is illustrated in Figure 1C. Together, Figure 1A-C show that, under Fisher's geometric model, the fitness of the F1 cross will depend on properties of the two parental lines, and properties of the chain of fixed effects that differentiate the lines. To determine the relevant properties, and their connections to the mode of divergence, we will sometimes consider the chains of homozygous and heterozygous effects, $2\mathbf{a}$ and $\mathbf{a} \pm \mathbf{d}$ (Figure 1B), and sometimes consider the chains of additive and dominance effects, $\mathbf{a}$ and $\mathbf{d}$ (Figure 1C).

1.1.2 Characterizing an arbitrary hybrid

The arguments above for the F1 cross generalize to an arbitrary hybrid (say, an F2 or a backcross). All possible hybrids will contain some subset of arrows shown in Figure 1. For this purpose, let J_1 be the subset of the D loci in the hybrid that are homozygous for the P1 allele, J_2 be the subset of the loci that are homozygous for the P2 allele, and J_{12} the subset of loci that are heterozygous. Since all divergent loci must be in one of these three states, any two of these sets can completely characterize the hybrid. This implies that the j-th trait value of any hybrid can be written in several equivalent ways, for example:

$$z_{\mathrm{H},j} = z_{\mathrm{P1},j} + \sum_{i \in J_2} 2a_{ij} + \sum_{i \in J_{12}} (a_{ij} + d_{ij}) \tag{6}$$

The size of these sets depends on the proportion of the divergent loci in the hybrid that are in each state (the two homozygotes and the heterozygote). Let us define these proportions via:

$$\begin{aligned} |J_1|/D &\equiv p_1 \\ |J_2|/D &\equiv p_2 \\ |J_{12}|/D &\equiv p_{12} \end{aligned} \tag{7}$$

Because all divergent loci must be one of these three states, we have:

$$p_1 + p_{12} + p_2 = 1 \tag{8}$$

Our aim in this paper is to calculate the expected fitness of a hybrid, conditional on its genome composition, i.e. conditional on p_1, p_1 and p_{12}. When we take expectations, they will be over the particular loci that are in any given state, e.g., over the particular Dp_{12} loci that are heterozygous. We then determine how this result depends on properties of $\mathbf{a}$ and $\mathbf{d}$ (the additive and dominance effects). Unlike previous work, we will derive these results exactly without making any assumptions about the distributions of these effects.

1.2 Expected log fitness of a hybrid

In the Methods, we show that the expected log fitness of the hybrid described in eq. 6 is:

$$\begin{aligned} E(\ln w_{\mathrm{H}}) = {} & p_1 \ln w_{\mathrm{P1}} + p_2 \ln w_{\mathrm{P2}} + p_{12} \ln w_{\mathrm{F1}} \\ & - p_1 p_2 \, f(2\mathbf{a}) \; - p_{12} p_1 \, f(\mathbf{a} + \mathbf{d}) \; - p_{12} p_2 \, f(\mathbf{a} - \mathbf{d}) \end{aligned} \tag{9}$$

where the function $f(\cdot)$ is defined as

$$f(\mathbf{x}) = \frac{D}{D-1}\left(\sum_{j=1}^{n}\sum_{i=1}^{D} x_{ij}^2 - \sum_{j=1}^{n}\left(\sum_{i=1}^{D} x_{ij}\right)^2\right) \tag{10}$$

Equation 9 contains six terms, each with a natural interpretation. The first three terms are simply a weighted sum of the log fitnesses of the three fixed genotypes: the two parents and the globally heterozygous F1. Because these terms contain fitness values, they can all vary with the position of the environmental optimum. As such, these three terms describe the extrinsic or environment-dependent component of expected hybrid fitness.

The second three terms do not vary with the position of the optimum, but only on the additive and dominance effects, i.e. on $\mathbf{a}$ and $\mathbf{d}$. As such, they describe the intrinsic, or environment-independent component of hybrid fitness. Each term describes interactions between heterospecific alleles in different states, and applies to a different type of substitution, corresponding to a different colour of arrow in Figure 1B. For example, the term $p_1 p_2 f\,(2\mathbf{a})$ describes interactions between homozygous P1 alleles and homozygous P2 alleles, and so it depends on the homozygous effects, $2\mathbf{a}$ (eq. 2; black arrows in Fig. 1B).

The next sections will explore the interpretation of these intrinsic fitness terms in detail. But first, let us note that eq. 9 can be rewritten in terms of the chains of additive and dominance effects and an interaction term (i.e., using the chains illustrated in Fig. 1C instead of those in Fig. 1B). In particular, we show in the Methods that eq. 9 is equivalent to

$$\begin{aligned} E\left(\ln w_{\mathrm{H}}\right) = {} & p_1 \ln w_{\mathrm{P1}} + p_2 \ln w_{\mathrm{P2}} + p_{12} \ln w_{\mathrm{F1}} \\ & - \left(p_1 p_{12} + p_2 p_{12} + 4 p_1 p_2\right) f\left(\mathbf{a}\right) \\ & - \left(p_1 p_{12} + p_2 p_{12}\right) f\left(\mathbf{d}\right) \\ & - \tfrac{1}{2} p_{12}(p_2 - p_1)\; g(\mathbf{a}, \mathbf{d}) \end{aligned} \tag{11}$$

where the function $g(\cdot,\cdot)$ is defined as

$$g(\mathbf{x}, \mathbf{y}) = 4\frac{D}{D-1}\left(\sum_{j=1}^{n}\sum_{i=1}^{D} x_{ij} y_{ij} - \sum_{j=1}^{n}\sum_{i=1}^{D} x_{ij} \sum_{k=1}^{D} y_{kj}\right) \tag{12}$$

such that $g(\mathbf{x}, \mathbf{x}) = 4f(\mathbf{x})$. Like eq. 9, eq. 11 includes three terms that determine intrinsic hybrid fitness. The first term, in $f(\mathbf{a})$, depends solely on the chain of additive effects (black arrows in Fig. 1C). This term includes interactions between loci in all possible combinations of the three states. The second intrinsic term, in $f(\mathbf{d})$, depends solely on the chain of dominance effects (purple arrows in Fig. 1C). This term includes only those interactions that involve loci in heterozygous state. The third term, in $g(\mathbf{a}, \mathbf{d})$, captures interactions between the additive and dominance effects. As we show below, it represents a form of directional dominance.

Let us also note that eq. 11 can be written in a more familiar form, which corresponds to the partition of Hill (1982), showing that the quantities $f(\mathbf{a})$, $f(\mathbf{d})$ and $g(\mathbf{a}, \mathbf{d})$ are estimable by standard quantitative genetic methods (Lynch, 1991; Lynch and Walsh, 1998, Ch. 9; Clo et al., 2021). The result follows from defining the hybrid index, $0 \leq h \leq 1$, as the total proportion of divergent sites that carry a P2 allele, such that:

$$h = p_2 + p_{12}/2 \tag{13}$$

With this definition, eq. 11 is equivalent to

$$
\begin{aligned}
E\left(\ln w_{\mathrm{H}}\right) = & \overline{\ln w_{\mathrm{P}}} \\
& + \left(h - \tfrac{1}{2}\right)\left(\ln w_{\mathrm{P2}} - \ln w_{\mathrm{P1}}\right) \\
& + p_{12}\left(\ln w_{\mathrm{F1}} - \overline{\ln w_{\mathrm{P}}}\right) \\
& - \left(4h(1-h) - p_{12}\right)\ f\left(\mathbf{a}\right) \\
& - p_{12}(1-p_{12})\ f\left(\mathbf{d}\right) \\
& - p_{12}\left(h - \tfrac{1}{2}\right)\ g(\mathbf{a}, \mathbf{d})
\end{aligned} \tag{14}
$$

where $\overline{\ln w_{\mathrm{P}}} = \frac{1}{2}\left(\ln w_{\mathrm{P2}} + \ln w_{\mathrm{P1}}\right)$ is the mean parental log fitness. Equation 14 is equivalent to the major result of Schneemann et al. (2020), where it was derived under the assumptions that the additive and dominance effects were characterized by universal pleiotropy, normality and statistical independence among traits. Here, we have shown that the result applies more generally, without any of these assumptions.

1.3 Interpretation of the intrinsic fitness terms

In this section, we consider the intrinsic fitness terms in eqs. 9, 11 and 14. Our aim is to connect the properties of the fixed effects, which result from the evolutionary divergence between the parental lines, to the outcomes of hybridization between the lines.

1.3.1 Directionality in the chains of effects

Above, we noted that each intrinsic term relates to a chain of fixed effects, as illustrated in Figure 1, and does so via the functions $f(\cdot)$ and $g(\cdot,\cdot)$. One way to understand these functions is to note that they capture the exchangeability of the substitutions, i.e. the extent to which different substitutions have similar effects. This can be parameterized in different ways (see, e.g., eq. 36), but one useful way captures the amount of "directionality" in the chain(s) of substitutions. To see this, let us note that eqs. 10 and 12 can also be written as (see Methods for details):

$$
f(\mathbf{x}) = \frac{D}{D-1}\sum_{i=1}^{D}\sum_{k=1,k\neq i}^{D} ||\mathbf{x}_i||||\mathbf{x}_k||\cos(\theta_{x_i,x_k}) \tag{15}
$$

$$
g(\mathbf{x},\mathbf{y}) = 4\frac{D}{D-1}\sum_{i=1}^{D}\sum_{k=1,k\neq i}^{D} ||\mathbf{x}_i||||\mathbf{y}_k||\cos(\theta_{x_i,y_k}) \tag{16}
$$

Here, $||\mathbf{x}_i||$ is the magnitude of a vector (i.e. the length of the arrow in Fig. 1) and θ_{x_i,x_k} is the angle between a pair of vectors (see Fig. 1B for an example). That is, we have $\cos(\theta) = -1$ when two substitutions point in the same phenotypic direction (such that $\theta = \pi$), $\cos(\theta) = 0$ when the vectors are orthogonal (e.g., altering the values of different traits) and $\cos(\theta) = 1$ for substitutions that point in opposite directions.

Together, eqs. 11, 15 and 16 allow us to draw strong connections between the mode of divergence, and the outcomes of hybridization. This is illustrated in Figure 2. Figure 2 reports individual-based simulations of Fisher's geometric model under six illustrative scenarios of divergence (all allopatric, and halted after $D = 25$ substitutions). As shown in the left-hand panels, scenarios I-IV each involve bouts of adaptive substitution, as one or both parental populations adapt to new optima; scenarios V-VI involve stabilizing selection, where both populations remained in environments with a single fixed optimum. Figure 2A-C show the consequences of these different modes of divergence for the intrinsic fitness of hybrids.

Additive effects. Figure 2A reports the values of $f(\mathbf{a})$, which depend on the additive effects, and which capture the intrinsic effects of admixture on hybrid fitness (eq. 14; Schneemann et al., 2020). From eq. 15, $f(\mathbf{a}) < 0$ should hold if the chain of additive effects mostly point in the same direction. This occurs under scenario I (blue box in Fig. 2A), where population P2 underwent direction selection towards a distant

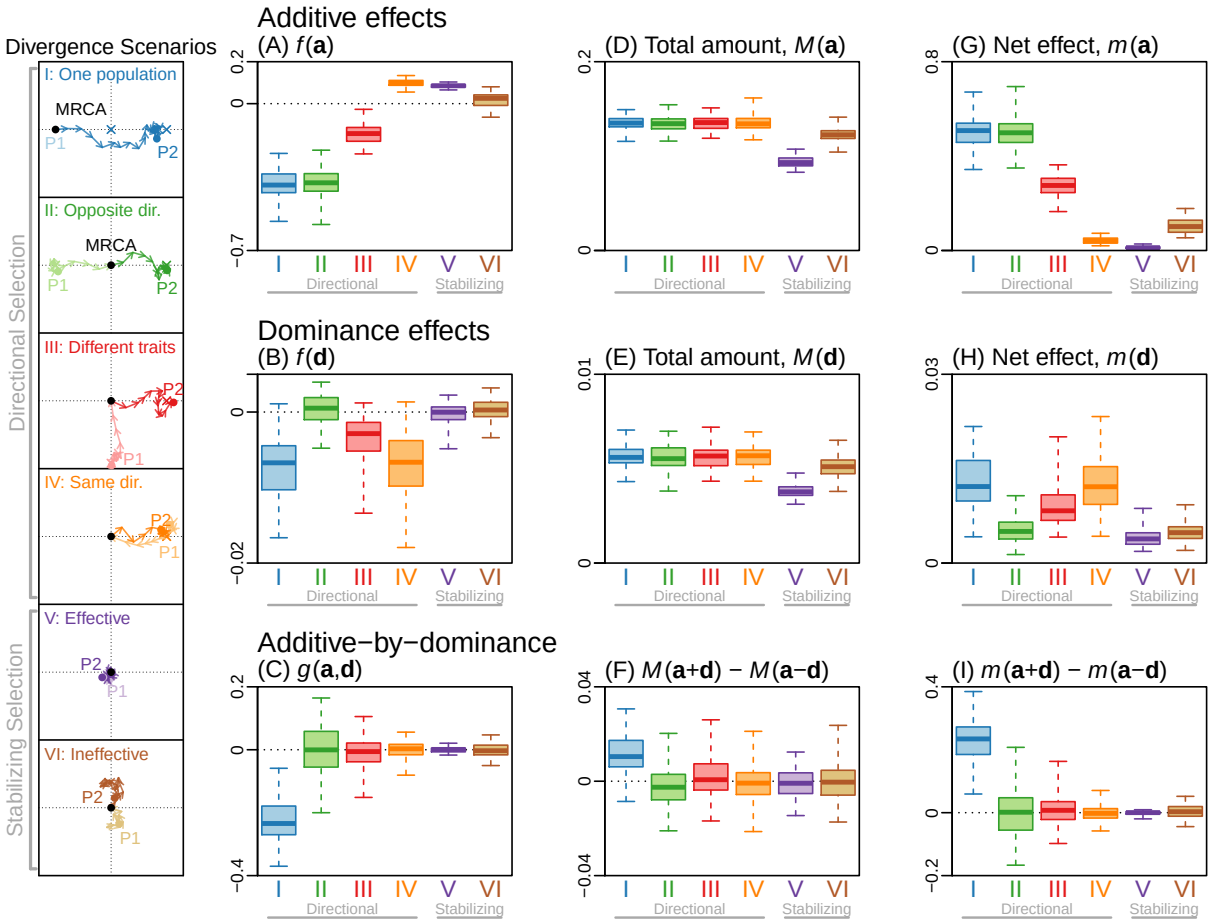

Figure 2: Divergence histories have predictable consequences for hybrid fitness under Fisher's geometric model. Illustrative individual-based simulations of divergence between two allopatric populations, each halted after $D = 25$ fixations. Simulations used six distinct scenarios of divergence, illustrated in the left-hand panels (see Methods for full details). Scenarios I-IV each involve directional selection, as one or both parental populations adapt to new optima. Scenarios V-VI each involve stabilizing selection, but in populations of different sizes ($N = 1000$ vs. $N = 10$). **(A)-(I)** Boxes represent results for 100 replicate simulations (median, quantiles and full range), and show various quantities relevant to hybrid fitness. **(A)-(C)** show the three quantities that appear in eqs. 11 and 14, and capture the intrinsic (environment-independent) effects on hybrid fitness. These quantities can also be decomposed into **(D)-(F)** the total amount of evolutionary change; and **(G)-(I)** the net effect of evolutionary change. These quantities vary predictably between the six scenarios, and do so in complementary ways for additive and dominance effects (see text).

.

optimum, while P1 remained in their ancestral state; it also occurs in scenario II (green box in Fig. 2A) where both populations adapted to new optima, but in opposite phenotypic directions. Results for scenarios I-II are identical because additive effects are defined with respect to the P1 genotype, not with respect to the ancestral state. If the two parental populations undergo directional selection on different traits (Scenario III: red box in Fig. 2A) then $f(\mathbf{a})$ is still negative but smaller, since $\cos(\theta) \approx -1$ for half of the pairs of substitutions and $\cos(\theta) \approx 0$ for the other half. By contrast, when natural selection tends to return the chain of additive effects to its starting point, then $\cos(\theta) > 0$ will hold on average, such that $f(\mathbf{a}) > 0$. This holds for scenario IV (where both parental lines adapted to a common optimum), and scenario V (where

the populations are under effective stabilizing selection). Finally, for scenario VI, we simulated a very small population ($N = 10$), such that stabilizing selection was ineffective. In this case, the parental lines wandered erratically in phenotypic space, such that $\cos(\theta) \approx 0$ on average, and $f(\mathbf{a})$ tends to vanish.

From the results above, and eqs. 11 or 14, it is clear that the history of divergence does have predictable consequences for the outcome of hybridization. When $f(\mathbf{a}) < 0$ (Scenarios I-III), then admixture between the parental lines will tend to increase hybrid fitness, creating the potential for beneficial heterosis (Schneemann et al., 2020). By contrast, when $f(\mathbf{a}) > 0$ (Scenarios IV-V), then admixture will tend to be deleterious, increasing RI between the parental lines. Finally, when $f(\mathbf{a}) \approx 0$ (Scenario VI), then admixture, per se, should have no net effect.

Dominance effects. Figure 2B shows equivalent results for $f(\mathbf{d})$, which capture the effects of phenotypic dominance on hybrid fitness. A key fact here is Haldane's Sieve – the tendency for directional selection to preferentially fix alleles that are dominant in the direction of selection (Haldane, 1924, 1927; Frankham, 1990; Crnokrak and Roff, 1995; Schneemann et al., 2022). This means that directionality in the dominance effects – unlike directionality in the additive effects – will depend on the MRCA. The result is that dominance effects and additive effects contain complementary information about the divergence history. To see this, note that scenarios I and II gave identical results for the additive effects (Fig. 2A), but give qualitatively different results for the dominance effects (Fig. 2B). This is because in scenario I, all dominance effects point from the MRCA towards the new optimum (to which P2 alone is adapted), and this directionality leads to strongly negative $f(\mathbf{d})$ (eq. 15). By contrast, in scenario II, adaptation took place in different directions with respect to the MRCA, and so the dominance effects also point in different directions, such that $f(\mathbf{d}) \approx 0$. Conversely, scenarios I and IV give very different results for their additive effects (Fig. 2A), but are identical with respect to their dominance effects (Fig. 2B); this is because in scenario IV, both populations adapted independently, but in the same direction (Mani and Clarke, 1990). Contrasting results for the additive and dominance effects are also observed under stabilizing selection (scenarios V-VI), although in this case, the explanation has nothing to do with Haldane's Sieve. The key fact here is that the additive effects are expressed together in the parental genotypes during the divergence process, but the dominance effects are not. It follows that selection cannot act to keep the dominance effects close to any optimum; so while the additive effects may be coadapted, the dominance effects will not be (Schneemann et al., 2022). This implies that the dominance effects may wander erratically in phenotypic space, such that $f(\mathbf{d}) \approx 0$.

Overall, then, the intrinsic effects of dominance will often be negligible, since $f(\mathbf{d}) \approx 0$ will often hold. Nevertheless, under certain forms of directional selection, when there has been net adaptation in a consistent phenotypic direction with respect to the MRCA, and where Haldane's Sieve has acted (Orr and Betancourt, 2001), then $f(\mathbf{d}) < 0$ can hold. In this case, hybrids with intermediate levels of heterozygosity can gain a fitness advantage (eq. 14).

Additive-by-dominance interaction. Finally, let us consider the interaction term, shown in Figure 2C. From eq. 16, $g(\mathbf{a}, \mathbf{d}) < 0$ will hold if the chains of additive effects and dominance effects tend to point in the same consistent direction, while $g(\mathbf{a}, \mathbf{d}) > 0$ will hold if these chains point in opposite directions. Of our six scenarios, such directionality arises only in scenario I, where both additive and dominance effects tend to point away from P1 (=MRCA) towards P2, such that $g(\mathbf{a}, \mathbf{d}) < 0$. This implies that, on average, P2 alleles are dominant over P1 alleles. Again, the consequences for hybrids are clear from eqs. 11 and 14. The dominance of the P2 alleles yields a net fitness benefit only if the homozygous loci also tend to carry P2 alleles (i.e., if $p_2 > p_1$, or, equivalently, if $h > 1/2$). Conversely, had P1 alleles tended to be dominant, then we would have $g(\mathbf{a}, \mathbf{d}) > 0$, and hybrids would gain an advantage if $p_2 < p_1$ or $h < 1/2$. In both cases, the explanation is that the dominance acts to preserve coadaptation between alleles from a single parent.

1.3.2 The total amount and net effect of evolutionary change

In the previous section, we described the key functions $f(\cdot)$ and $g(\cdot, \cdot)$ in terms of the directionality in the chains of substitutions (eqs. 15-16). We can gain further insight by writing eq. 10 as follows:

$$f(\mathbf{x}) = \frac{D}{D-1}(M(\mathbf{x}) - m(\mathbf{x})) \tag{17}$$

where

$$M(\mathbf{x}) \equiv \sum_i^D \|\mathbf{x}_i\|^2 \quad \text{and} \quad m(\mathbf{x}) \equiv \left\| \sum_i^D \mathbf{x}_i \right\|^2 . \tag{18}$$

Here, we have defined two functions: $M(\cdot)$ is the sum of the squared magnitudes of the set of vectors, and $m(\cdot)$ is the squared magnitude of the sum of vectors. For substitution effects (Figure 1) these two functions have a natural interpretation, and capture different properties of the evolutionary divergence.

In particular, $M(\cdot)$ captures the *total amount of evolutionary change*. For additive effects, we have

$$M(\mathbf{a}) = \sum_i^D \|\mathbf{a}_i\|^2 \tag{19}$$

so any factor leading to more substitutions, or to larger substitutions, will increase the total amount of evolutionary change. As shown by previous authors, the relevant factors are legion, and include the pattern of environmental change (e.g. Kopp and Hermisson, 2009; Matuszewski et al., 2014; Yamaguchi and Otto, 2020), and all of the standard population genetic parameters (see, e.g., Supplementary Figure S1). As shown in Figure 2D, the values of $M(\mathbf{a})$ were identical for our scenarios I-IV. This is because all of these scenarios involved two comparable bouts of directional selection, and so the typical sizes of the substitutions ($\|\mathbf{a}_i\|$), as well as their number ($D = 25$) were the same in all cases. The total amount of change was smaller when substitutions were driven by drift (Scenario VI), and especially when stabilizing selection was effective (Scenario V), because mutations of smaller size tended to fix. As shown in Figure 2E, the same pattern was evident in $M(\mathbf{d})$, the total amount of evolutionary change in the dominance effects.

By contrast, $m(\cdot)$ captures *the net effect of the evolutionary change*, and depends on the differences between phenotypes after the divergence has taken place. For additive effects, we have

$$m(\mathbf{a}) = \left\| \sum_i^D \mathbf{a}_i \right\|^2 = \left\| \mathbf{z}_{\mathrm{P1}} - \frac{\mathbf{z}_{\mathrm{P2}} + \mathbf{z}_{\mathrm{P1}}}{2} \right\|^2 = \frac{1}{4} \|\mathbf{z}_{\mathrm{P2}} - \mathbf{z}_{\mathrm{P1}}\|^2 \tag{20}$$

which depends on the difference in the parental phenotypes (see the black dotted line in Figure 1C). It follows that $m(\mathbf{a})$ will be largest in cases of divergent selection (Schluter, 2000), and will correspond to the differences between the new parental optima. This is confirmed by results in Figure 2G (Scenarios I-IV). When environmental conditions are shared, $m(\mathbf{a})$ will depend on the ability of populations to track their optima – i.e. on the efficacy of phenotypic selection. With stabilizing selection (Figure 2G, scenarios V-VI) this is closely related to the mutation-drift load. As shown by previous authors, this load also varies in predictable ways with the full suite of population-genetic parameters (e.g., Hartl and Taubes, 1996; Poon and Otto, 2000; Zhang and Hill, 2003; Tenaillon et al., 2007; Lourenço et al., 2011; Roze and Blanckaert, 2014; see also Supplementary Figure S1). For the dominance effects, the net effect of evolutionary change is

$$m(\mathbf{d}) = \left\| \sum_i^D \mathbf{d}_i \right\|^2 = \left\| \mathbf{z}_{\mathrm{F1}} - \frac{\mathbf{z}_{\mathrm{P2}} + \mathbf{z}_{\mathrm{P1}}}{2} \right\|^2 \tag{21}$$

which is the distance between the midparent and the F1 (see the purple dotted line in Figure 1C). Because the F1 is not under selection during the divergence, its phenotype can evolve erratically, but the net effect

of change will also be influenced by directional dominance, resulting from past selection (Schneemann et al., 2022). This is all confirmed in Figure 2H.

Finally, the additive-by-dominance interaction can be written as the difference between the total amounts and net effects of evolutionary change, for the two sets of heterozygous effects. In other words, it depends on the differences between the red and blue paths illustrated in Figure 1B. In particular, we can write

$$\begin{aligned} g(\mathbf{a},\mathbf{d}) &= f(\mathbf{a}+\mathbf{d}) - f(\mathbf{a}-\mathbf{d}) \\ &= \frac{D}{D-1}\left[\{M(\mathbf{a}+\mathbf{d}) - M(\mathbf{a}-\mathbf{d})\} - \{m(\mathbf{a}+\mathbf{d}) - m(\mathbf{a}-\mathbf{d})\}\right] \end{aligned} \tag{22}$$

As shown in Figure 2F and 2I, for scenarios II-VI, there was no systematic difference between the two chains of effects. This applied to both the total amounts of change (Fig. 2F); and the net effects of change (Fig. 2I). For scenario I, by contrast, P2 alleles were more dominant, because only the P2 lineage underwent directional selection. This meant that the heterozygous effects of the P2 alleles were larger ($M(\mathbf{a}+\mathbf{d}) > M(\mathbf{a}-\mathbf{d})$; Fig. 2F), and that their combined effect on the phenotype was also larger ($m(\mathbf{a}+\mathbf{d}) > m(\mathbf{a}-\mathbf{d})$; Fig. 2I).

1.3.3 Definition in terms of fitness effects

The quantities $M(\cdot)$ and $m(\cdot)$, which describe the total amount, and net effect of evolutionary change, can also be represented in terms of fitness, rather than phenotypes. This implies that they are measurable in principle, even when the phenotypic model is not taken literally (Martin, 2014). To see this, let us consider the homozygous fitness effects (equivalent results can be simply derived for the heterozygous effects). Now, let s_i denote the deleterious fitness effect of inserting a single homozygous substitution i into an otherwise optimal background, so that

$$s_i \approx -\ln(1-s_i) = \sum_{j=1}^{n} (2a_{ij})^2 \tag{23}$$

If $\bar{s}$ denotes the mean of these effects for all D substitutions, then we have:

$$M(2\mathbf{a}) = -\sum_{i}^{D} \ln(1-s_i) \approx D\bar{s} \tag{24}$$

So $M(2\mathbf{a})$ will be large if the parental lines have fixed many mutations with large fitness effects. By contrast, $m(2\mathbf{a})$ describes the fitness effect of adding all of the divergent alleles at once into an otherwise optimal genotype. This is equal to the sum of the individual fitness effects, plus their pairwise epistatic interactions (noting that all interactions are pairwise with the model of eq. 1; Martin et al., 2007). If we define s_{ik} as the fitness effect of inserting a given pair of substitutions into an optimal background, then the pairwise epistatic effect is

$$\begin{aligned} \epsilon_{ik} &\equiv \ln(1-s_{ik}) - \ln(1-s_i) - \ln(1-s_k) \\ &= -8\sum_{j=1}^{n} a_{ij}a_{kj}. \end{aligned} \tag{25}$$

(e.g. Martin et al., 2007). Equation 25 shows that the sign of the fitness epistasis relates to the tendency of mutations to point in the same direction (Fraïsse and Welch, 2019). With these definitions, it follows that

$$m(2\mathbf{a}) = |\ln w_{\mathrm{P2}} - \ln w_{\mathrm{P1}}|\,, \qquad \text{if } \ln w_{\mathrm{P1}} = 0 \text{ or } \ln w_{\mathrm{P2}} = 0 \tag{26}$$

$$= -\sum_{i}^{D} \ln(1-s_i) - \tfrac{1}{2}\sum_{i=1}^{D}\sum_{k=1,k\neq i}^{D} \epsilon_{ik}$$

$$\approx D\bar{s} - \tfrac{1}{2}D(D-1)\bar{\epsilon} \tag{27}$$

So even if $M(2\mathbf{a})$ is very large, $m(2\mathbf{a})$ can remain small if there is positive fitness epistasis between the substitutions ($\bar{\epsilon} > 0$), such that the two lines have similar levels of fitness in any given environment. This might be so, for example, if the divergence comprised mildly deleterious mutations, alongside compensatory beneficial mutations.

Note that $M(2\mathbf{a}) = m(2\mathbf{a})$ when there is no epistasis on average ($\bar{\epsilon} = 0$), as would be the case if the populations accumulated randomly-orientated mutations (Martin et al., 2007; Simon et al., 2018; Fraïsse and Welch, 2019; see scenario VI in Figure 2). Indeed it follows generally, that $f(2\mathbf{a}) = D^2\bar{\epsilon}/2$, so that this key function is a measure of fitness epistasis. It follows too that epistasis is maximally negative when all substitutions have identical individual effects, in which case $\epsilon = -2s$.

Let us note here that the net effect of evolutionary change can sometimes be related to the fitness of the initial F1 cross, assumed here to be fully heterozygous (Schneemann et al., 2022). For example, if dominance effects are negligible ($\mathbf{d} \approx \mathbf{0}$), then the F1 matches the midparent, and we have $\ln w_{\mathrm{F1}} = \overline{\ln w_{\mathrm{P}}} + m(\mathbf{a})$, while if the midparent is close to optimal, then we have $\ln w_{\mathrm{F1}} = -m(\mathbf{d})$ (Fig. 1C; Schneemann et al., 2022).

1.4 Intrinsic versus extrinsic isolation

In this section, we show that $M(2\mathbf{a})$ and $m(2\mathbf{a})$ can also govern the strengths of intrinsic versus extrinsic RI. To see this, let us consider the case of divergent selection and local adaptation (Schluter, 2000; Yamaguchi and Otto, 2020), where the parental lines have adapted to different environments, A and B, characterized by different phenotypic optima. For simplicity and brevity, we will assume that the two parental populations are well adapted to their respective optima, and assume that phenotypes are additive, such that $\mathbf{d} = \mathbf{0}$. With these assumptions, the net effect of the evolutionary divergence is the same as the squared difference between the optima (i.e. $m(2\mathbf{a}) = ||\mathbf{o}_A - \mathbf{o}_B||^2$), and the fitnesses of the three fixed genotypes are:

	Environment A	Environment B
$\ln w_{\mathrm{P1}}$	0	$-m(2\mathbf{a})$
$\ln w_{\mathrm{P2}}$	$-m(2\mathbf{a})$	0
$\ln w_{\mathrm{F1}}$	$-m(2\mathbf{a})/4$	$-m(2\mathbf{a})/4$

The fitness of the F1 is the same in both environments because, with our assumptions, its phenotype will be exactly intermediate between the two optima (at a distance $\sqrt{m(2\mathbf{a})}/2$ from either). Now we can write the expected hybrid fitness in the two environments solely in terms of $M(2\mathbf{a})$ and $m(2\mathbf{a})$. Results are simplest if we assume that genomic divergence is high, such that $D/(D-1) \approx 1$. In this case, from eq. 14 we find:

$$E\left(\ln w_H\right) \approx \begin{cases} -M(2\mathbf{a})\left(h(1-h) - p_{12}/4\right) - m(2\mathbf{a})h^2, & \text{In environment } A \\ -M(2\mathbf{a})\left(h(1-h) - p_{12}/4\right) - m(2\mathbf{a})(1-h)^2, & \text{In environment } B \end{cases} \tag{28}$$

This result shows clearly that $M(2\mathbf{a})$ and $m(2\mathbf{a})$ cause RI of different kinds. The term weighted by $M(2\mathbf{a})$ is identical in environment A and environment B. Therefore, the total amount of evolutionary change determines the strength of intrinsic RI, where hybrids are disfavoured in either environment. By contrast, the term weighted by $m(2\mathbf{a})$ determines the strength of extrinsic RI. The net effect of evolutionary change

determines how far P1-like hybrids (with low h) are favoured in environment A, and disfavoured in environment B. The relative importance of these two terms is therefore determined by the ratio $M(2\mathbf{a})/m(2\mathbf{a})$. This is illustrated in Figure 3. Figure 3A-B shows the expected log fitness of various hybrids (namely the F2 and reciprocal backcrosses) in each environment. When the ratio $M(2\mathbf{a})/m(2\mathbf{a})$ is small (orange curves in Fig. 3A-B) then the maladapted parental type is the least fit genotype, and hybrids are intermediate. Hybrid fitness is determined largely by the hybrid index (i.e. the extent to which hybrids resemble P1 or P2), and heterozygosity has little impact on the results. As a result, the F2 (in the centre of each plot) has similar fitness to the F1 (shown by the black crosses). By contrast, when the ratio $M(2\mathbf{a})/m(2\mathbf{a})$ is large (green curves in Fig. 3A-B), the position of the optimum has much less effect on the results. Hybrids of all kinds are selected against in both environments. When the ratio takes an intermediate value (blue curves in Fig. 3A-B), there is a mix of intrinsic and extrinsic effects.

The results above capture one major way in which the history of environmental change affects the evolution of RI (Yamaguchi and Otto, 2020). They also show that results depend not only on the environmental change, but also on the nature of the populations' genetic response to this change. To see this, let us note that the total amount of evolutionary change can be written as:

$$M(2\mathbf{a}) = \frac{T^2}{D}(1 + CV^2) \tag{29}$$

where

$$T \equiv \sum_{i=1}^{D} 2\,\|\mathbf{a_i}\| \tag{30}$$

is the total length of the phenotypic trajectory covered by the evolving populations (i.e. the sum of the lengths of all of the black arrows shown in Fig. 1A-B) and CV is the coefficient of variation in the magnitudes of the substitutions (i.e. the standard deviation of the arrow lengths, divided by their mean). Orr (1998) showed that when populations adapt to a distant optimum, then the distribution of magnitudes is often close to exponential, such that $CV \approx 1$.

This all implies that $M(2\mathbf{a})$ will be large if populations adapted to their new optima via a relatively long phenotypic trajectory (large T). This might occur, for example, if the ancestral environment was characterized by a very different phenotypic optimum. $M(2\mathbf{a})$ would be especially large if the populations followed this trajectory by fixing a few very large-effect mutations (small D). Such a case is illustrated by the green arrows in Figure 3C, which leads to the pattern of intrinsic isolation shown in Fig. 3A-B. By contrast, $M(2\mathbf{a})$ will be small if populations adapted to their new optima via a relatively short phenotypic trajectory (small T). This might occur, for example, if environment A was also the shared ancestral environment of the two populations. $M(2\mathbf{a})$ would be especially small if the populations followed this trajectory by fixing a large number of small-effect substitutions (large D). Such a case is illustrated by the orange arrows in Figure 3C, which result in the pattern of extrinsic isolation shown in Fig. 3A-B. Finally, it is also clear that identical patterns of RI can arise in different ways. For example, the blue lines in Fig. 3A-B (like all other outcomes) might have been achieved by a short phenotypic trajectory, tracked by a few large-effect mutations (blue arrows in Fig. 3C), or by a longer phenotypic trajectory, tracked by many small-effect mutations (blue arrows in Fig. 3D).

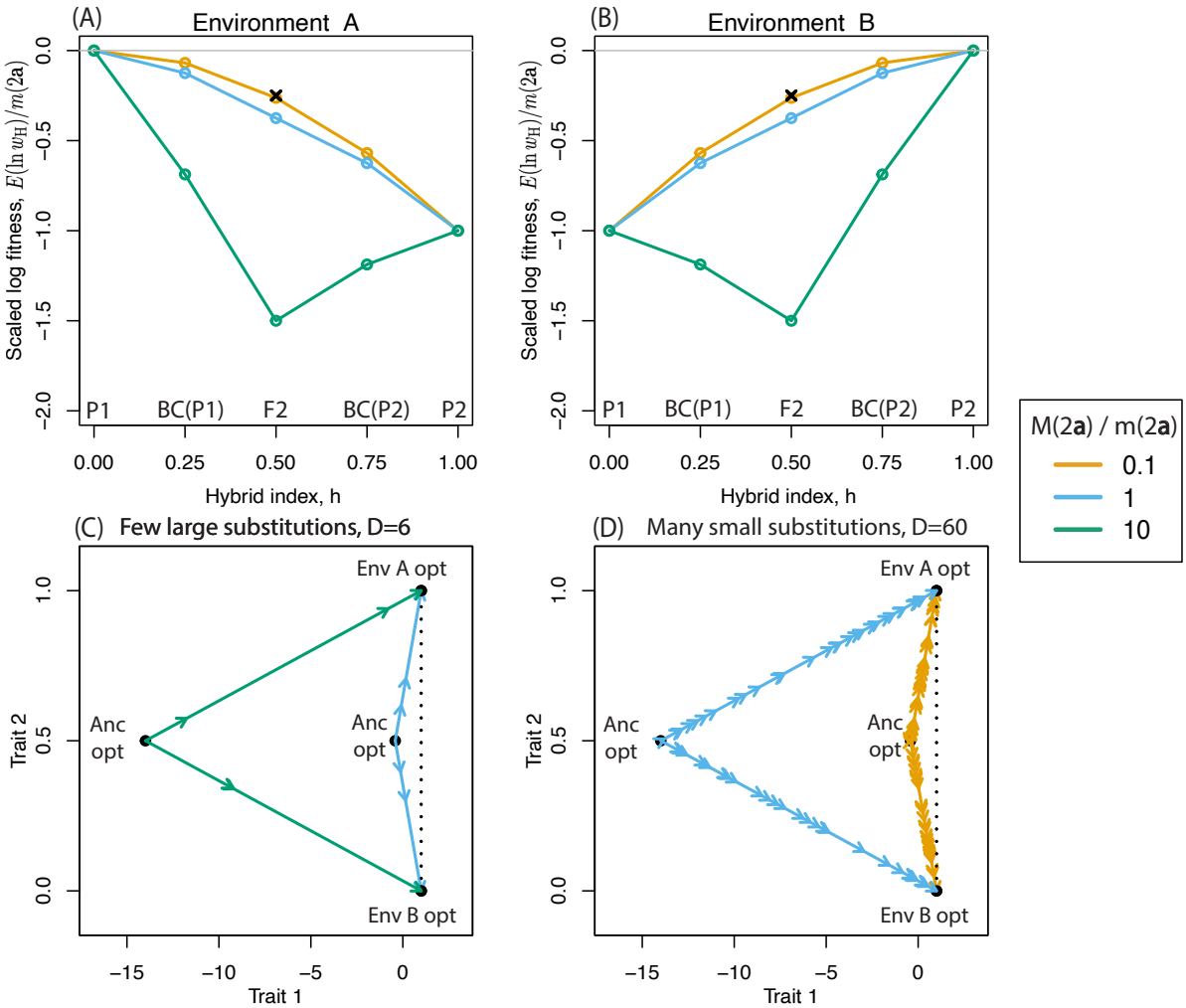

Figure 3: The divergence history can affect the relative strengths of intrinsic and extrinsic reproductive isolation. Assuming the parental populations are well adapted to their respective optima, eq. 28 shows that hybrid fitness is dependent on the ratio of $M(2\mathbf{a})$ (the total amount of evolutionary change) to $m(2\mathbf{a})$ (the net effect of evolutionary change). **(A)-(B)**: the scaled expected log fitness of various hybrids in the two parental environments. Illustrated are the parental types (P1: $h = p_{12} = 0$; P2: $h = 1$, $p_{12} = 0$), the reciprocal backcrosses (BC(P1): $h = 1/4$, $p_{12} = 1/2$; BC(P2): $h = 3/4$, $p_{12} = 1/2$) and the second-generation hybrid (F2: $h = p_{12} = 1/2$). The black cross shows the initial F1 hybrid ($h = 1/2$, $p_{12} = 1$). **(C)-(D)** Different divergence histories can lead to predictably different outcomes. Intrinsic isolation is most likely to result from large phenotypic trajectories, covered in a few large substitutions (green arrows), whereas purely extrinsic isolation is most likely to result from short phenotypic trajectories, covered in many small-effect substitutions (orange arrows). But the same patterns of RI can also result from different divergence histories (blue arrows), as long as they yield the same ratio $M(2\mathbf{a})/m(2\mathbf{a})$.

2 Discussion

This work has explored how the mode of divergence between parental populations impacts the fitness of their hybrids, and thus the extent of reproductive isolation. This can be framed in two ways: what can we learn about the (unobserved) history of parental divergence by observing their hybrids? (Welch, 2004; Schneemann et al., 2020; Fraser, 2020); and conversely, which divergence scenarios will predictably lead to RI? (Coyne and Orr, 2004). The latter question is essential for understanding the opposing processes of speciation and adaptive introgression (Abbott et al., 2013), and predicting the outcomes of novel hybridizations, including those that are human-mediated (Genovart, 2008; Chan et al., 2019).

We have examined the connections between divergence and hybrid fitness using a simple fitness landscape model, which is also relatable to phenotypic data (Fisher, 1930; Orr, 1998; Martin, 2014); and have focused on results most likely to yield simple, testable predictions. As a result, we have considered only the expected hybrid fitness (eqs. 9, 11 and 14), and not the variance or higher moments, since the latter will be qualitatively affected by the recombination map and environmental variance. We have also neglected factors such as phenotypic epistasis, and directional plasticity, which are certain to affect outcomes, but not (yet) in a predictable way (Stamp and Hadfield, 2020).

Finally, we have used a simple quadratic model of fitness (eq. 1) which precludes higher-order fitness interactions (Martin et al., 2007; Fraïsse et al., 2016), even though such interactions are often observed in cross data (Fraïsse et al., 2014; Fraïsse and Welch, 2019). Nevertheless, results here apply more broadly if fitness values can be suitably transformed (Simon et al., 2018; Schneemann et al., 2020).

With these caveats, we have shown that the outcome of hybridization can be predicted from summary statistics of the fixed effects that differentiate the populations, as captured by the function $f(\cdot)$ (eq. 10). This quantity can be further decomposed into two other quantities which are simpler to understand, and which we have called the "total amount of evolutionary change", $M(\cdot)$, and "net effect of evolutionary change", $m(\cdot)$ (eq. 18). If the history of environmental change, or the population genetic parameters, have predictable effects on hybridization outcomes (Chevin et al., 2014; Yamaguchi and Otto, 2020; Schneemann et al., 2020, 2022), then they do so via these two quantities.

Because results depend solely on these quantities, it follows directly that very different histories of evolutionary divergence can yield identical patterns of hybrid fitness. Nevertheless, we have shown that some information about the divergence history is present (Figure 2), and that the additive and dominance effects contain complementary information. Under stabilizing selection, the difference arises because additive effects will tend to be coadapted, while dominance effects will not (Schneemann et al., 2022). Under directional selection, the difference comes because additive effects trace the phenotypic path between the parents, while dominance effects point in the direction of past selection (i.e., from the MRCA) – the effect known as Haldane's Sieve (Haldane, 1924, 1927; Frankham, 1990; Crnokrak and Roff, 1995). Of course, this additional information about the divergence history will only be present if Haldane's Sieve has acted, which may not be so if adaptation starts from standing variation (Orr and Betancourt, 2001).

Our results also have implications for the relative contributions of large- and small-effect loci to the outcomes of hybridization. On one hand, our results imply that identical patterns of RI can arise from a few large-effect substitutions or many small-effect substitutions. This means that the presence or absence of large-effects, without further information, tells us little about the overall amount or pattern of RI. On the other hand, the total amount of evolutionary change is defined as the sum of *squared* effect sizes (eq. 18). It follows, therefore, that the same amount of phenotypic change will result in a larger $M(2\mathbf{a})$ if the change took place with fewer but larger substitutions (eqs. 29-30; Fig. 3C-D).

Finally, our results also have implications, which were not explored here, for the stability of local adaptation, and the evolution of genetic architectures (Dekens et al., 2021; Yeaman, 2022). For example, the dominance of alleles may be a major determinant of the effective rates of migration between demes, and the possibility of allele swamping (Barton, 1992). Directional dominance, resulting from local adaptation, may therefore act as a source of asymmetric gene flow between derived and ancestral populations (see, e.g., Fig. 2C). Similarly, a large body of previous work suggests that the architecture of adaptation will be affected by the presence or absence of gene flow (Yeaman, 2022). In particular, adaptation in the face of gene flow should create architectures that are more "concentrated", i.e., involving fewer, larger effects, and tighter linkage.

Combined with results here, this implies that ongoing gene flow during local adaptation might sometimes increase the strength of resulting intrinsic RI (Fig. 3).

3 Methods

3.1 Derivation of main result

We want to derive the log fitness, or the squared Euclidean distance, of a hybrid to the optimum. That is, we want

$$E(\ln w_H) = E(-||z_H - o||^2) = -E\left(\sum_{j=1}^{n}(z_{H,j} - o_j)^2\right) = -\sum_{j=1}^{n} E((z_{H,j} - o_j)^2)$$

For the remainder of this subsection, we will focus on a single trait j and drop the subscript j for brevity.

$$\begin{aligned}
E((z_{H,j} - o_j)^2) = E((z_H - o)^2) = E\left(\left(z_{\mathrm{P1}} - o + 2\sum_{i\in J_{22}} a_i + \sum_{k\in J_{12}}(a_k + d_k)\right)^2\right) \\
= E\Bigg((z_{\mathrm{P1}} - o)^2 + 4\left(\sum_{i\in J_{22}} a_i\right)^2 + \left(\sum_{i\in J_{12}} a_i\right)^2 + \left(\sum_{i\in J_{12}} d_i\right)^2 \\
+ 2(z_{\mathrm{P1}} - o)\left(2\sum_{i\in J_{22}} a_i + \sum_{k\in J_{12}}(a_k + d_k)\right) \\
+ 2\sum_{i\in J_{12}} a_i \sum_{k\in J_{12}} d_k + 4\sum_{i\in J_{22}} a_i \sum_{k\in J_{12}}(a_k + d_k)\Bigg)
\end{aligned} \tag{31}$$

In these expressions, the expectations are not over the additive and dominance effects, but over the particular set of loci that are homozygous and heterozygous in the hybrid. That is, they are over the sets J_{22} and J_{12}. To obtain expectations over these sets, we define indicator functions.

$$I_J(i) = \begin{cases} 1 \text{ if } i \in J \\ 0 \text{ otherwise} \end{cases}$$

We can then use these functions as follows:

$$\begin{aligned}
E\left(\sum_{i\in J} x_i\right) = E\left(\sum_{i=1}^{D} x_i I_J(i)\right) = \sum_{i=1}^{D} x_i E\left(I_J(i)\right) \\
= \sum_{i=1}^{D} x_i P(i \in J) = \frac{|J|}{D}\sum_{i=1}^{D} x_i \\
\equiv \frac{|J|}{D} S_x
\end{aligned}$$

where $|J|$ is the size of the set. We have introduced the notation

$$S_{x,j} \equiv \sum_{i=1}^{D} x_{i,j}$$

Let us also introduce

$$S_{xy,j} \equiv \sum_{i=1}^{D} x_{i,j} y_{i,j}$$

For both, we again leave out the subscript j for simplicity for the remainder of this section.

For the square and cross-terms in eq. 31, we use the same approach.

$$\begin{aligned}
E\left(\sum_{i\in J} x_i \sum_{k\in J} y_k\right) &= E\left(\sum_{i=1}^{D}\sum_{k=1}^{D} x_i y_k I_J(i) I_J(k)\right) \\
&= \sum_{i=1}^{D} x_i y_i P(i \in J) + \sum_{i=1}^{D}\sum_{k=1,k\neq i}^{D} x_i y_k P(i \in J \cap k \in J) \\
&= \frac{|J|}{D}\sum_{i=1}^{D} x_i y_i + \frac{|J|\,(|J|-1)}{D(D-1)}\sum_{i=1}^{D}\sum_{k=1,k\neq i}^{D} x_i y_k \\
&= \frac{|J|\,S_{xy}}{D} + \frac{|J|\,(|J|-1)}{D(D-1)}\left(S_x S_y - S_{xy}\right) \\
&= \frac{|J|\,(D-|J|)}{D(D-1)}\left(S_{xy} - S_x S_y\right) + \frac{|J|}{D} S_x S_y
\end{aligned}$$

and similarly

$$\begin{aligned}
E\left(\sum_{i\in J} x_i \sum_{k\in K} y_k\right) &= \sum_{i=1}^{D}\sum_{k=1,k\neq i}^{D} x_i y_k P(i \in J \cap k \in K) \\
&= \frac{|J|\,|K|}{D(D-1)}\sum_{i=1}^{D}\sum_{k=1,k\neq i}^{D} x_i y_k \\
&= \frac{|J|\,|K|}{D(D-1)}\left(S_x S_y - S_{xy}\right)
\end{aligned}$$

Now we can combine these results, with eqs. 7 and 31. After some algebra, we obtain

$$\begin{aligned}
E((z_H - o)^2) = {} & (z_{\mathrm{P1}} - o)^2 + 2(z_{P1} - o)((2p_2 + p_{12})S_a + p_{12}S_d) \\
& + 4p_2 S_a^2 + p_{12}S_a^2 + p_{12}S_d^2 + 2p_{12}S_a S_d \\
& + (4p_2(1-p_2) + p_{12}(1-p_{12}) - 4p_2 p_{12})\,\frac{D}{D-1}\left(S_{aa} - S_a^2\right) \\
& + p_{12}(1-p_{12})\frac{D}{D-1}\left(S_{dd} - S_d^2\right) \\
& + (2p_{12}(1-p_{12}) - 4p_2 p_{12})\,\frac{D}{D-1}\left(S_{ad} - S_a S_d\right)
\end{aligned} \tag{32}$$

We note that, given some n, d, p_{12} and p_2, there will be a total of

$$\binom{d}{dp_{12}}\binom{d(1-p_{12})}{dp_2} = \frac{d!}{(dp_1)!(dp_2)!(dp_{12})!}$$

possible hybrids, each with equal probability, so in theory one could write out the complete discrete probability distribution function for the hybrid fitness over all possible hybrids in a given situation. One can also compute arbitrary moments using the same indicator function approach as above.

3.2 Rearrangement of main result

Let us now derive eq. 9 from the above. We will start with the first two lines of equation 32. Recall that in the section above, we were working in a single dimension corresponding to trait j, and had dropped the subscript. We re-introduce it here. Our equation is therefore

$$\begin{aligned}
E\left(\sum_{j=1}^{n}(z_{H,j}-o_j)^2\right) &= \sum_{j=1}^{n} E((z_{H,j}-o_j)^2 \\
&= \sum_{j=1}^{n} \ (z_{\mathrm{P}1,j}-o_j)^2 + 2(z_{P1,j}-o_j)((2p_2+p_{12})S_{a,j}+p_{12}S_{d,j}) \\
&+ 4p_2S_{a,j}^2 + p_{12}S_{a,j}^2 + p_{12}S_{d,j}^2 + 2p_{12}S_{a,j}S_{d,j} \\
&+ (4p_2(1-p_2)+p_{12}(1-p_{12})-4p_2p_{12})\,\frac{D}{D-1}\left(S_{aa,j}-S_{a,j}^2\right) \\
&+ p_{12}(1-p_{12})\frac{D}{D-1}\left(S_{dd,j}-S_{d,j}^2\right) \\
&+ (2p_{12}(1-p_{12})-4p_2p_{12})\,\frac{D}{D-1}\left(S_{ad,j}-S_{a,j}S_{d,j}\right)
\end{aligned} \tag{33}$$

We first note that, from eqs. 2 and 3, we have

$$z_{\mathrm{P}2,j} = z_{\mathrm{P}1,j} + 2S_{a,j} \quad \text{and} \quad z_{\mathrm{F}1,j} = z_{\mathrm{P}2,j} + S_{a,j} + S_{d,j}$$

It therefore follows that:

$$\begin{aligned}
-(p_1 \ln w_{\mathrm{P}1} + p_2 \ln w_{\mathrm{P}2} + p_{12} \ln w_{\mathrm{F}1}) &= \sum_{j=1}^{n} p_1(z_{\mathrm{P}1,j}-o_j)^2 + p_2(z_{\mathrm{P}2,j}-o_j)^2 + p_{12}(z_{\mathrm{F}1,j}-o_j)^2 \\
&= \sum_{j=1}^{n} p_1(z_{\mathrm{P}1,j}-o_j)^2 + p_2(z_{\mathrm{P}1,j}-o_j+2S_{a,j})^2 + p_{12}(z_{\mathrm{P}1,j}-o_j+S_{a,j}+S_{d,j})^2 \\
&= \sum_{j=1}^{n}(z_{\mathrm{P}1,j}-o_j)^2 + 2(z_{P1,j}-o_j)((2p_2+p_{12})S_{a,j}+p_{12}S_{d,j}) + 4p_2S_{a,j}^2 \\
&\qquad + p_{12}S_{a,j}^2 + p_{12}S_{d,j}^2 + 2p_{12}S_{a,j}S_{d,j}
\end{aligned}$$

which corresponds to the first few lines of the expected hybrid fitness in equation 33.

For the remaining terms in Equation 33, we use the definition

$$f(\mathbf{x}) = \frac{D}{D-1}\left(\sum_{j=1}^{n}\sum_{i=1}^{D} x_{ij}^2 - \sum_{j=1}^{n}\left(\sum_{i=1}^{D} x_{ij}\right)^2\right) = \frac{D}{D-1}\sum_{j=1}^{n}\left(S_{xx,j}-S_{x,j}^2\right)$$

Notice that

$$
\begin{aligned}
f(2\mathbf{a}) &= 4f(\mathbf{a}) \\
f(\mathbf{a}+\mathbf{d}) &= f(\mathbf{a}) + f(\mathbf{d}) + 2\frac{D}{D-1}\sum_{j=1}^{n}(S_{ad,j} - S_{a,j}S_{d,j}) \\
f(\mathbf{a}-\mathbf{d}) &= f(\mathbf{a}) + f(\mathbf{d}) - 2\frac{D}{D-1}\sum_{j=1}^{n}(S_{ad,j} - S_{a,j}S_{d,j}) \\
f(\mathbf{a}+\mathbf{d}) + f(\mathbf{a}-\mathbf{d}) &= 2f(\mathbf{a}) + 2f(\mathbf{d})
\end{aligned}
$$

Using this, one can show an equivalence with the last three lines of equation 32.

$$
\begin{aligned}
&p_1p_2f(2\mathbf{a}) + p_{12}p_1f(\mathbf{a}+\mathbf{d}) + p_{12}p_2f(\mathbf{a}-\mathbf{d}) \\
&\quad = \sum_{j=1}^{n}\left(4p_2(1-p_2) + p_{12}(1-p_{12}) - 4p_2p_{12}\right)\frac{D}{D-1}\left(S_{aa,j} - S_{a,j}^2\right) \\
&\quad + p_{12}(1-p_{12})\frac{D}{D-1}\left(S_{dd,j} - S_{d,j}^2\right) \\
&\quad + \left(2p_{12}(1-p_{12}) - 4p_2p_{12}\right)\frac{D}{D-1}\left(S_{ad,j} - S_{a,j}S_{d,j}\right)
\end{aligned}
$$

Altogether this gives Equation 9. We can also derive Equation 11 from here; the easiest way to see the equivalence is to set $g(\mathbf{a},\mathbf{d}) = f(\mathbf{a}+\mathbf{d}) - f(\mathbf{a}-\mathbf{d})$ (as shown below) in Equation 11, collect terms with the coefficient $p_{12}(1-p_{12})$, and set $f(\mathbf{a}+\mathbf{d}) + f(\mathbf{a}-\mathbf{d}) = 2f(\mathbf{a}) + 2f(\mathbf{d})$ as shown above.

3.3 Representations of the functions $f(\cdot)$ and $g(\cdot,\cdot)$

We can write the functions $f(\cdot)$ and $g(\cdot,\cdot)$ in several different ways. Simplest is equation 17, which follows directly from eq. 10 in the main text. We can also write both functions in terms of cosine similarities and magnitudes of the vectors using the definition of dot product and the cosine rule. Notice that

$$
\left\|\sum_{i}^{D}\mathbf{x}_i\right\|^2 = \left(\sum_{i=1}^{D}\mathbf{x}_i\right)\cdot\left(\sum_{i=1}^{D}\mathbf{x}_i\right) = \sum_{i=1}^{D}\mathbf{x}_i\cdot\mathbf{x}_i + \sum_{i=1}^{D}\sum_{k=1,k\neq i}^{D}\mathbf{x}_i\cdot\mathbf{x}_k \tag{34}
$$

$$
= \sum_{i=1}^{D}||\mathbf{x}_i||^2 - \sum_{i=1}^{D}\sum_{k=1,k\neq i}^{D}||\mathbf{x}_i||||\mathbf{x}_k||\cos(\theta_{x_i,x_k}) \tag{35}
$$

where θ_{x_i,x_k} is the angle between the ith and the kth substitution vectors in the chain (e.g. see Figure 1B), by the definition of dot product, and where the negative sign comes from the need to take the supplementary angle due to the directionality of the vectors. This is effectively a generalized cosine law, and yields Equation 15 directly. Equation 16 follows in the same way, as follows:

$$
\begin{aligned}
g(\mathbf{a},\mathbf{d}) &= f(\mathbf{a}+\mathbf{d}) - f(\mathbf{a}-\mathbf{d}) \\
&= \frac{4D}{D-1}\sum_{j=1}(S_{ad,j} - S_{a,j}S_{d,j}) \\
&= \frac{4D}{D-1}\sum_{j=1}^{n}\left(\sum_{i=1}^{D} a_{ij}d_{ij} - \sum_{i=1}^{D}\sum_{k=1}^{D} a_{ij}d_{kj}\right) \\
&= \frac{-4D}{D-1}\sum_{i=1}^{D}\sum_{k=1,k\neq i}^{D}\sum_{j=1}^{n} a_{ij}d_{kj} = \frac{-4D}{D-1}\sum_{i=1}^{D}\sum_{k=1,k\neq i}^{D} \mathbf{a}_i\cdot\mathbf{d}_k \\
&= \frac{4D}{D-1}\sum_{i=1}^{D}\sum_{k=1,k\neq i}^{D} ||\mathbf{a}_i||||\mathbf{d}_k||\cos(\theta_{a_i,d_k})
\end{aligned}
$$

Here, again, θ_{x_i,y_k} is the angle between the substitution vectors x_i and y_k, by the definition of dot product, and where the sign switch in the last line comes from the need to take the supplementary angle due to the directionality of the vectors.

These representation of $f(\cdot)$ and $g(\cdot,\cdot)$ in terms of cosine similarities and vector magnitudes are only one way of capturing the amount of exchangeability between the fixed differences. We can also use the following relationship between the dot product and the squared Euclidean distance:

$$
2\mathbf{x}_i\cdot\mathbf{x}_k = ||\mathbf{x}_i||^2 + ||\mathbf{x}_k||^2 - ||\mathbf{x}_i - \mathbf{x}_k||^2
$$

which, with results above, yields:

$$
\begin{aligned}
f(\mathbf{x}) &= -\frac{1}{2}\frac{D}{D-1}\sum_{i=1}^{D}\sum_{k=1,k\neq i}^{D}\left(||\mathbf{x}_i||^2 + ||\mathbf{x}_k||^2 - ||\mathbf{x}_i - \mathbf{x}_k||^2\right) \\
&= \frac{D}{D-1}\sum_{i=1}^{D-1}\sum_{k=i+1}^{D}\left(||\mathbf{x}_i - \mathbf{x}_k||^2 - ||\mathbf{x}_i||^2 - ||\mathbf{x}_k||^2\right) \\
&= \frac{D}{D-1}\sum_{i=1}^{D-1}\sum_{k=i+1}^{D} ||\mathbf{x}_i - \mathbf{x}_k||^2 - D\ M(\mathbf{x}) \qquad (36)
\end{aligned}
$$

which shows clearly that, for a given amount of evolutionary change, i.e. a fixed $M(\mathbf{x})$, $f(\mathbf{x})$ is minimized when all substitutions have identical effects.

Lastly, we can write $f(\mathbf{x})$ in terms of the moments of the substitution vectors, so as to connect more clearly to the result given in Schneemann et al. (2020). In particular, defining the sample mean and variance on trait j as

$$
\mu_j = \frac{1}{D}\sum_{i=1}^{D} x_{ij} \qquad (37)
$$

$$
\sigma_j^2 = \frac{D}{D-1}\left(\frac{1}{D}\sum_{i=1}^{D} x_{ij}^2 - \frac{1}{D^2}\left(\sum_{i=1}^{D} x_{ij}\right)^2\right) \qquad (38)
$$

so that we can write

$$
\begin{aligned}
f(\mathbf{x}) &= \frac{D}{D-1}\left(\sum_{j=1}^{n}\sum_{i=1}^{D} x_{ij}^2 - \sum_{j=1}^{n}\left(\sum_{i=1}^{D} x_{ij}\right)^2\right) \\
&= \frac{D^2}{D-1}\sum_{j=1}^{n}\left(\sigma_j^2 - (D-1)\mu_j^2\right) \qquad (39)
\end{aligned}
$$

Equation 39 provides a way to understand $f(\mathbf{x})$ in the context of moments on each trait. In particular, it describes the effects of segregation variance on a trait-by-trait basis. When applied to the additive effects $\mathbf{a}$, for example, it shows that these effects are captures by the sample variances and means of the additive effects. Note that this expression contains no covariances, but it applies whether or not the additive effects do covary between traits.

Simulations

The illustrative simulations shown in Figure 2 calculated new quantities from runs reported previously by Schneemann et al. (2022) (and which were themselves based on the simulation methods reported in Schneemann et al., 2020). While full details are reported in these papers, briefly, simulations were individual-based, and used pairs of allopatric, diploid Wright-Fisher populations, each comprising either $N = 1000$ (scenarios I-V) or $N = 10$ (scenario VI) simultaneous hermaphrodites, with discrete non-overlapping generations. Every generation, parents were selected with a probability proportional to their fitness (as calculated from eq. 1) with $n = 20$ traits under selection. Gametes were generated from the parental genomes with free recombination among all sites, and mutation. For mutation, a Poisson-distributed number, with mean $2NU$, of mutations were randomly assigned to unique sites, and we set $U = 0.01$. The n homozygous effects for each new mutation were drawn from a multivariate normal distribution with vanishing mean and covariances, and a common variance set such that the mean deleterious effects of a mutation in an optimal background was $\bar{s}_{\text{mut}} = 0.01$. The dominance effect of each mutation on each trait was set at its additive effect multiplied by a shifted beta-distributed random number with vanishing mode, median and mean (implying additivity on average), bounds at -1 and 1 (complete recessivity or dominance) and variance 1/6 (see Figure 2 of Schneemann et al., 2022). After a total of $D = 25$ substitutions had fixed across both populations, the two parental genotypes were chosen as the genotypes containing only the fixed effects in each population. For scenarios I-IV, one or both populations were placed in environments where the optimum on one of the n traits was at a distance of $\sqrt{1/2}$ away from the shared ancestral state. This led to an initial bout of adaptive substitution, as populations adapted to their new optima. For scenario I, this procedure was repeated twice for population P2, while for scenarios II-IV, both populations adapted to new optima, displaced from the MRCA either in opposite directions (scenario II), or on different traits (scenario III), or in the same direction (scenario IV). For scenarios V-VI, the optima were set equal to the shared ancestral state, and substitutions accumulated via system drift (Schiffman and Ralph, 2021). The two-trait cartoons in the left-hand panels of Figure 2 are solely to illustrate these scenarios. All simulation results are reported in Supplementary Table 1.

Acknowledgements

B.D.S. and H.S. acknowledge support from the Wellcome Trust program in Mathematical Genomics and Medicine (WT220023 and RG92770).

References

Abbott, R., Albach, D., Ansell, S., Arntzen, J. W., Baird, S. J. E., Bierne, N., Boughman, J., Brelsford, A., Buerkle, C. A., Buggs, R., Butlin, R. K., Dieckmann, U., Eroukhmanoff, F., Grill, A., Cahan, S. H., Hermansen, J. S., Hewitt, G., Hudson, A. G., Jiggins, C., Jones, J., Keller, B., Marczewski, T., Mallet, J., Martinez-Rodriguez, P., Möst, M., Mullen, S., Nichols, R., Nolte, A. W., Parisod, C., Pfennig, K., Rice, A. M., Ritchie, M. G., Seifert, B., Smadja, C. M., Stelkens, R., Szymura, J. M., Väinölä, R., Wolf, J. B. W., and Zinner, D. (2013). Hybridization and speciation. *Journal of Evolutionary Biology*, 26(2):229–246.

Arnold, M. L. and Hodges, S. A. (1995). Are natural hybrids fit or unfit relative to their parents? *Trends in Ecology & Evolution*, 10(2):67–71.

Barton, N. H. (1992). On the spread of new gene combinations in the third phase of Wright's shifting-balance. *Evolution*, 46(2):551–557.

Barton, N. H. (2001). The role of hybridization in evolution. *Molecular Ecology*, 10(3):551–568.

Bernardes, J. P., Stelkens, R. B., and Greig, D. (2017). Heterosis in hybrids within and between yeast species. *Journal of Evolutionary Biology*, 30(3):538–548.

Bierne, N., Gagnaire, P.-A., and David, P. (2013). The geography of introgression in a patchy environment and the thorn in the side of ecological speciation. *Current Zoology*, 59(1):72–86.

Chan, W. Y., Hoffmann, A. A., and Oppen, M. J. H. (2019). Hybridization as a conservation management tool. *Conservation Letters*, 12(5).

Chevin, L.-M., Decorzent, G., and Lenormand, T. (2014). Niche dimensionality and the genetics of ecological speciation. *Evolution*, 68(5):1244–1256.

Clo, J., Ronfort, J., and Gay, L. (2021). Fitness consequences of hybridization in a predominantly selfing species: insights into the role of dominance and epistatic incompatibilities. *Heredity*, 127(4):393–400.

Coughlan, J. M. and Matute, D. R. (2020). The importance of intrinsic postzygotic barriers throughout the speciation process. *Philosophical Transactions of the Royal Society B: Biological Sciences*, 375(1806):20190533.

Coyne, J. A. and Orr, H. A. (2004). *Speciation*, volume 1. Oxford University Press.

Crnokrak, P. and Roff, D. A. (1995). Dominance variance: Associations with selection and fitness. *Heredity*, 75(5):530–540.

Dekens, L., Otto, S. P., and Calvez, V. (2021). The best of both worlds: combining population genetic and quantitative genetic models.

Edmands, S. (1999). Heterosis and outbreeding depression in interpopulation crosses spanning a wide range of divergence. *Evolution*, 53(6):1757–1768.

Edmands, S. (2002). Does parental divergence predict reproductive compatibility? *Trends in Ecology & Evolution*, 17(11):520–527.

Fisher, R. A. (1930). *The genetical theory of natural selection.* Clarendon Press.

Frankham, R. (1990). Are responses to artificial selection for reproductive fitness characters consistently asymmetrical? *Genetical Research*, 56(1):35–42.

Fraser, H. B. (2020). Detecting selection with a genetic cross. *Proceedings of the National Academy of Sciences*, 117(36):22323–22330.

Fraïsse, C., Elderfield, J. A. D., and Welch, J. J. (2014). The genetics of speciation: are complex incompatibilities easier to evolve? *Journal of Evolutionary Biology*, 27(4):688–699.

Fraïsse, C., Gunnarsson, P. A., Roze, D., Bierne, N., and Welch, J. J. (2016). The genetics of speciation: Insights from Fisher's geometric model. *Evolution*, 70(7):1450–1464.

Fraïsse, C. and Welch, J. J. (2019). The distribution of epistasis on simple fitness landscapes. *Biology Letters*, 15(4):20180881.

Genovart, M. (2008). Natural hybridization and conservation. *Biodiversity and Conservation*, 18(6):1435–1439.

Haldane, J. B. S. (1924). A mathematical theory of natural and artificial selection, Part I. *Transactions of the Cambridge Philosophical Society*, 23:19–41.

Haldane, J. B. S. (1927). A mathematical theory of natural and artificial selection, Part V: selection and mutation. *Mathematical Proceedings of the Cambridge Philosophical Society*, 28:838–844.

Hartl, D. and Taubes, C. (1996). Compensatory nearly neutral mutations: Selection without adaptation. *Journal of Theoretical Biology*, 182(3):303–309.

Hill, W. G. (1982). Dominance and epistasis as components of heterosis. *Zeitschrift für Tierzüchtung und Züchtungsbiologie*, 99(1-4):161–168.

Jezkova, T., Leal, M., and Rodríguez-Robles, J. A. (2013). Genetic drift or natural selection? hybridization and asymmetric mitochondrial introgression in two caribbean lizards (anolis pulchellus and anolis krugi). *Journal of Evolutionary Biology*, 26(7):1458–1471.

Kopp, M. and Hermisson, J. (2009). The genetic basis of phenotypic adaptation II: The distribution of adaptive substitutions in the moving optimum model. *Genetics*, 183(4):1453–1476.

Lourenço, J., Galtier, N., and Glémin, S. (2011). Complexity, pleiotropy and the fitness effects of mutations. *Evolution*, 65(6):1559–1571.

Lynch, M. (1991). The genetic interpretation of inbreeding depression and outbreeding depression. *Evolution*, 45(3):622–629.

Lynch, M. and Walsh, B. (1998). *Genetics and analysis of quantitative traits*. Sinauer, Sunderland, Mass.

Mani, G. and Clarke, B. (1990). Mutational order: a major stochastic process in evolution. *Proceedings of the Royal Society of London. B. Biological Sciences*, 240(1297):29–37.

Martin, G. (2014). Fisher's geometrical model emerges as a property of complex integrated phenotypic networks. *Genetics*, 197(1):237–255.

Martin, G., Elena, S. F., and Lenormand, T. (2007). Distributions of epistasis in microbes fit predictions from a fitness landscape model. *Nature Genetics*, 39(4):555–560.

Martin, G. and Lenormand, T. (2006). The fitness effect of mutations across environments: A survey in light of fitness landscape models. *Evolution*, 60(12):2413.

Matuszewski, S., Hermisson, J., and Kopp, M. (2014). Fisher's geometric model with a moving optimum. *Evolution*, 68(9):2571–2588.

Moran, B. M., Payne, C., Langdon, Q., Powell, D. L., Brandvain, Y., and Schumer, M. (2021). The genomic consequences of hybridization. *eLife*, 10.

Orr, H. A. (1998). The population genetics of adaptation: The distribution of factors fixed during adaptive evolution. *Evolution*, 52(4):935–949.

Orr, H. A. and Betancourt, A. J. (2001). Haldane's sieve and adaptation from the standing genetic variation. *Genetics*, 157(2):875–884.

Poon, A. and Otto, S. P. (2000). Compensating for our load of mutations: Freezing the meltdown of small populations. *Evolution*, 54(5):1467–1479.

Roze, D. and Blanckaert, A. (2014). Epistasis, pleiotropy, and the mutation load in sexual and asexual populations. *Evolution*, 68(1):137–149.

Satokangas, I., Martin, S. H., Helanterä, H., Saramäki, J., and Kulmuni, J. (2020). Multilocus interactions and the build-up of reproductive isolation. *Philosophical Transactions of the Royal Society B: Biological Sciences*, 375(1806):20190543.

Schiffman, J. S. and Ralph, P. L. (2021). System drift and speciation. *Evolution*, 76(2):236–251.

Schluter, D. (2000). *The ecology of adaptive radiation*. Oxford University Press.

Schluter, D. and Conte, G. L. (2009). Genetics and ecological speciation. *Proceedings of the National Academy of Sciences*, 106(Supplement_1):9955–9962.

Schneemann, H., Munzur, A. D., Thompson, K. A., and Welch, J. J. (2022). The diverse effects of phenotypic dominance on hybrid fitness. *bioRxiv*.

Schneemann, H., Sanctis, B. D., Roze, D., Bierne, N., and Welch, J. J. (2020). The geometry and genetics of hybridization. *Evolution*, 74(12):2575–2590.

Simon, A., Bierne, N., and Welch, J. J. (2018). Coadapted genomes and selection on hybrids: Fisher's geometric model explains a variety of empirical patterns. *Evolution Letters*, 2(5):472–498.

Stamp, M. A. and Hadfield, J. D. (2020). The relative importance of plasticity versus genetic differentiation in explaining between population differences a meta-analysis. *Ecology Letters*, 23(10):1432–1441.

Tenaillon, O., Silander, O. K., Uzan, J.-P., and Chao, L. (2007). Quantifying organismal complexity using a population genetic approach. *PLoS ONE*, 2(2):e217.

Thompson, K. A., Urquhart-Cronish, M., Whitney, K. D., Rieseberg, L. H., and Schluter, D. (2021). Patterns, predictors, and consequences of dominance in hybrids. *The American Naturalist*, 197(3).

Welch, J. J. (2004). Accumulating Dobzhansky-Muller incompatibilities: reconciling theory and data. *Evolution*, 58(6):1145–1156.

Yamaguchi, R. and Otto, S. P. (2020). Insights from Fisher's geometric model on the likelihood of speciation under different histories of environmental change. *Evolution*, 74(8):1603–1619.

Yeaman, S. (2022). Evolution of polygenic traits under global vs local adaptation. *Genetics*, 220(1).

Zhang, X.-S. and Hill, W. G. (2003). Multivariate stabilizing selection and pleiotropy in the maintenance of quantitative genetic variation. *Evolution*, 57(8):1761–1775.

Supplementary figures

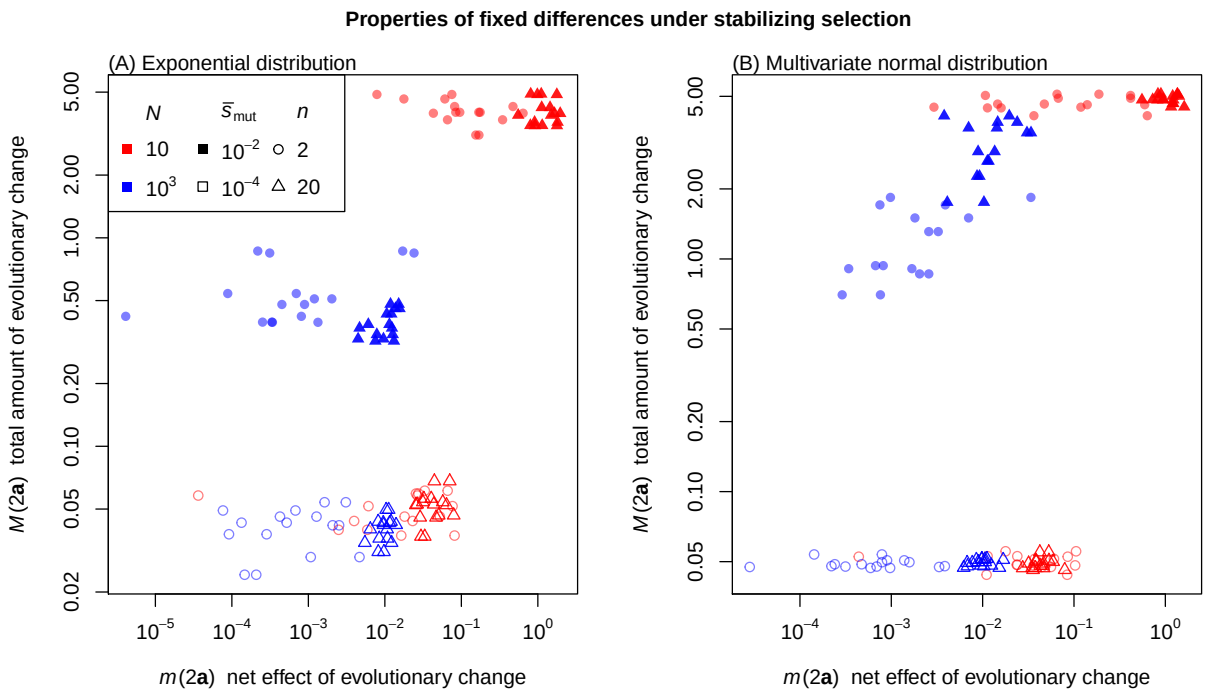

Figure S1: The total amount and net effect of evolutionary change under stabilizing selection. Under a common evolutionary scenario, the key quantities described in this work will vary with the population genetic parameters. To see this, the total amount of evolutionary change, $M(2\mathbf{a})$, and the net effect of evolutionary change, $m(2\mathbf{a})$, were calculated from the simulation runs reported by Schneemann et al. (2020). Each panel shows results from 128 simulated populations, using a fully crossed set of population-genetic parameters, each replicated twice. Varied were the population size (N: red versus blue points), the mean selection coefficient of a new mutation in an optimal background ($\bar{s}_{\text{mut}}$: filled versus unfilled points); and the number of phenotypic traits (n: circular versus triangular points). Also varied were the genomic mutation rates: $U \in \{0.01, 0.001, 0.0001, 0.00001\}$, and the rates of recombination. For recombination, we used either a single chromosome with map length one Morgan, and Haldane's mapping function, such that the mean crossover fraction was $\bar{c} \approx 0.216$; or free recombination among all loci, such that $\bar{c} = 0.5$. Neither mutation nor recombination rates had a qualitative effect in the parameter regimes simulated, and so they are not indicated visually. **(A)** shows results when the magnitudes of new mutations were drawn from an exponential distribution, with a random orientations in n-dimensional space; **(B)** shows results when the mutational effect on each trait was drawn from an i.i.d. normal distribution. In all cases, the phenotypic model was additive ($\mathbf{d} = \mathbf{0}$), and simulations were halted after $D = 500$ substitutions had fixed. Individual simulation results are reported in Supplementary Table 2.